Immersed AC electrospray (iACE) for monodispersed aqueous droplet generation

Zehao Pan, Yongfan Men, Satyajyoti Senapati, and Hsueh-Chia Chang

Citation: Biomicrofluidics **12**, 044113 (2018); doi: 10.1063/1.5048307
View online: https://doi.org/10.1063/1.5048307
View Table of Contents: http://aip.scitation.org/toc/bmf/12/4
Published by the American Institute of Physics

Immersed AC electrospray (iACE) for monodispersed aqueous droplet generation

Zehao Pan,[1] Yongfan Men,[2] Satyajyoti Senapati,[1] and Hsueh-Chia Chang[1]
[1]*Center for Microfluidics and Medical Diagnostics, Department of Chemical and Biomolecular Engineering, University of Notre Dame, Notre Dame, 46556 Indiana, USA*
[2]*Shenzhen Institutes of Advanced Technology, Chinese Academy of Sciences, Shenzhen, Guangdong 518055, China*

(Received 12 July 2018; accepted 7 August 2018; published online 16 August 2018)

We report a new immersed alternating current (AC) electrospray droplet generation method that can generate monodispersed water-in-oil droplets, with diameters ranging from 5 μm to 150 μm, in a stationary oil phase. This method offers high through-put, easy size tuning, and droplets with a viscous aqueous phase at high ionic strengths (raw physiological samples). Yet, it does not require coordinated flows of the dispersed/continuous phases or even a microfluidic chip. The design relies on a small constant back pressure (less than 0.1 atm) to drive the water phase through a nozzle (glass micropipette) and a non-isotropic AC electric Maxwell pressure to eject it into the oil phase. Undesirable field-induced discharge and nanojet formation at the tip are suppressed with a biocompatible polymer, polyethylene oxide. Its viscoelastic property favors the monodispersed dripping mechanism, with a distinct neck forming at the capillary tip before pinch-off, such that the tip dimension is the only controlling length scale. Consecutive droplets are connected by a whipping filament that disperses the drops away from the high-field nozzle to prevent electro-coalescence. A scaling theory is developed to correlate the droplet size with the applied pressure, the most important tuning parameter, and to determine the optimum frequency. The potential applications of this technology to biological systems are demonstrated with a digital loop-mediated isothermal amplification experiment, with little damage to the nucleic acids and other biomolecules, but with easy adaptive tuning for the optimum droplet number for accurate quantification. *Published by AIP Publishing.* https://doi.org/10.1063/1.5048307

I. INTRODUCTION

In recent years, monodispersed water-in-oil emulsion has seen a wide range of applications in biochemical assays, digital polymerase chain reaction (PCR), single cell analysis, gel coating/encapsulation of cells, and material synthesis.[1–5] Since the early 2000s, microfluidic methods based on hydrodynamic shear have allowed high-throughput generation of monodispersed emulsion. Such methods, which include T-junction,[6] coflow,[7,8] and flow focusing,[9,10] require two precisely controlled streams of water and oil phases. The droplet size can be tuned by adjusting the flow rate ratio of the two streams, which is quite laborious due to a multitude of parallel-flow viscous, inertial, and capillary hydrodynamic instabilities. Such well-controlled high-pressure streams with a high shear rate can only be realized in robust microfluidic chips. A specially designed pumping system with good flow control is needed for prolonged experiments, as syringe pumps tend to fluctuate over time and require long initiation times.[11] Finally, the high oil flow rate enhances the hydrodynamic interaction between neighboring nozzles, and scaling up to multiple droplet-generating modules requires separate microfluidic channels. Hence, there is considerable room for improvement in user friendliness, production cost, and scale-up.

An electric field is often used in combination with the various shear-based microfluidic methods to exert additional control over the droplet dispersing process.[12–15] In fact, electrospray can eject droplets independently, without the shearing action of a continuous-phase flow. As

such, it does not need to be housed within a microfluidic chip.[16] Immersed electrospray in an immiscible continuous phase has been reported by several authors.[17–19] It relies solely on an electric field and a single dispersed-phase flow to eject femtoliter droplets with a Taylor cone in the discharge mode. Since the electrospray setup does not require accurate flow control and coordination, the method could potentially be developed into a chip-free miniaturized device with a massive number of nozzles and without moving parts (electromagnetic vibrator).[20] However, electrospray cannot produce monodispersed droplets without an external shearing flow because of electric discharge and field-induced droplet coalescence.[21] Field-induced coalescence is particularly problematic in oil, as its high viscosity prevents dispersion of the ejected droplets in the high-field region near the nozzle. In fact, droplet generation by an immersed electrospray in a static continuous phase has been described as a chaotic process because of the discharge and coalescence events.[22,23]

In this paper, we report a novel droplet generation mechanism using an immersed alternating current (AC) electrospray (iACE) setup that can generate monodispersed droplets from 25 μm to 100 μm in diameter, with a coefficient of variation (CV) below 5%. Discharge instability due to high surface charge density in conventional direct current (DC) electrospray is suppressed by using a high-frequency AC field, which induces a low interfacial charge density when the AC frequency is close to the inverse RC time of the nozzle.[24,25] The inverse RC time is defined as $D/d\lambda$, where d is the diameter of the tip related to the length of the conducting electrolyte resistor and λ is the Debye length connected to the Debye layer capacitor on the droplet interface. Prevention of droplet coalescence is achieved with viscoelastic and biocompatible additives, such as PEO (polyethylene oxide), in the dispersed phase. The viscoelastic additives suppress Taylor cone formation and delay the droplet pinching to the end of a whipping filament that can disperse the droplets without coalescence. In iACE, the droplet size can be controlled by tuning the applied pressure and nozzle tip diameter. The droplet generation throughput (frequency) of a single iACE nozzle is comparable to the current microfluidic emulsification methods.

Loop-mediated isothermal amplification (LAMP) is increasingly being used in point-of-care applications such as virus detection[26,27] due to its constant reaction temperature, high specificity, and sensitivity. To demonstrate the utility of iACE, we performed absolute nucleic acid quantification using digital loop-mediated isothermal amplification (digital LAMP)[28] on lambda DNA as a model system. Other than demonstrating the viability of our droplet generation technology for LAMP—that the AC field does not degrade the molecular analytes and reagents, our new droplet generation technology also offers a major advantage for digital droplet PCR and LAMP. Digital PCR is often used for absolute quantification of specific DNA (and to a lesser degree RNA) copy number. Quite often, the pathogen number (and hence the copy number of their genomic DNA or RNA) in physiological samples can vary over a large dynamic range (six orders of magnitude).[29] To get accurate quantification, the number of droplets needs to be adjusted, and so, it is roughly at least one fifth of the copy number. As the sample volume remains the same, this requires iterations on the droplet size. The fact that our droplet generation technology allows easy adjustment of droplet size will greatly simplify this adaptive iteration process.

II. EXPERIMENTAL SECTION

A. Fabrication of micropipettes

Glass capillaries with an inner diameter (ID) of 0.78 mm and an outer diameter (OD) of 1 mm were purchased from Harvard Apparatus (Cambridge, MA). The capillaries were pulled into micropipettes using a pipette puller P-2000 (Sutter, Novato, CA) with a four line program. Line 1: heat 350, filament 4, velocity 50, delay 225, and pull 0; line 2: heat 350, filament 4, velocity 50, delay 225, and pull 0; line 3: heat 350, filament 4, velocity 50, delay 225, and pull 0; and line 4: heat 350, filament 4, velocity 50, delay 126, and pull 20. The program produced conic-shaped micropipettes with the tip diameter ranging from 3 μm to 8 μm. The pulled micropipettes were then etched with 10% hydrogen fluoride (HF) solution while applying a constant

air pressure from its base. No gas bubble will come out of the pipette tip until the applied pressure can overcome the capillary pressure which is determined by the tip diameter. After air bubbles began to emerge from its tip, the micropipettes were transferred into deionized water to wash off the remnant HF solution. The tip diameter can be tuned by adjusting the back pressure during etching. After drying out any water on the micropipettes, they were vapor primed by hexamethyldisilazane (HMDS) to prevent wetting during droplet generation.

B. Experimental setup

A cylindrical reservoir with a tube fitting on its side wall was attached to an indium tin oxide (ITO) coated glass substrate, as shown in Fig. 1(a). The ITO coated side served as the counter electrode in the droplet generation system and was connected to the ground. The micropipette was inserted through the fitting into the reservoir so that its tip is around 10 mm away from the inner wall of the reservoir. The inner diameter of the fitting was matched with the outer diameter of the micropipette so that the distance between the micropipette and the counter electrode was kept constant at 12 mm. Once a micropipette was inserted, wax was used to seal the gap between the micropipette and the fitting [not shown in Fig. 1(a)]. A reservoir can be used multiple times with different micropipettes. Power was supplied through an electrode (aluminum wire) inserted into the micropipette immersed in the aqueous phase. Alternating current was generated from a function generator (Agilent 33220A, Santa Clara, CA) and amplified by a step-up transformer (Model 113737, Industrial Test Equipment, Port Washington, NY). All AC voltage mentioned in this report represents the root mean square voltage. The AC frequency was fixed at 10 kHz in all experiments. DC power was supplied using a high voltage DC power supply (Matsusada, Charlotte, NC). Air pressure on the aqueous phase was controlled with a pressure regulator. After a micropipette was properly placed, the dispersed phase was filled through its base side and automatically wetted its inner wall until the meniscus reached the tip. After the oil phase was added to the reservoir, the aqueous/oil interface can be fixed within the micropipette by applying a small back pressure before the droplet generation. Images and videos were taken with a CCD camera (Retiga EXi, QImaging) connected to a microscope. A high

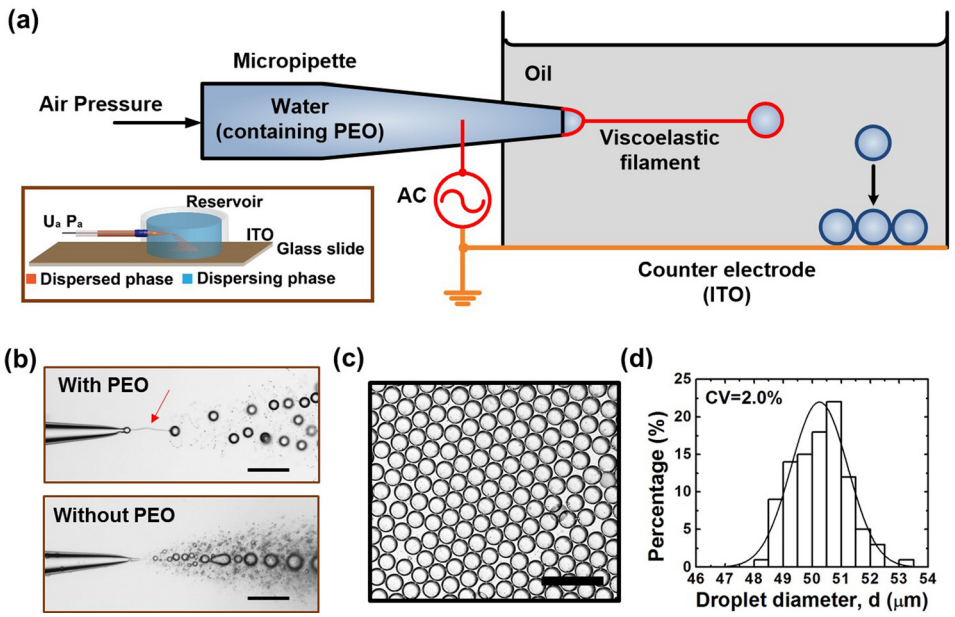

FIG. 1. (a) Schematic image of the experimental setup and 3D rendering of the experimental setup. (b) Snapshots of iACE in operation with or without 1%PEO as the dispersed phase. The arrow points to the viscoelastic filament as the meniscus pinches off. The ejected droplets formed a double helix as a result of the winding filament spiral. The scale bar is 200 μm. (c) Monolayer of water-in-oil droplets at the bottom of the reservoir. The scale bar is 200 μm. (d) The histogram of the droplet diameter shown in (c).

speed video was taken with a smartphone (iPhone8, Apple Inc., Cupertino, CA) mounted on the microscope at 240 fps. The oil phase was isopropyl palmitate (Sigma-Aldrich, St. Louis, MO) and contained 7% (w/w) surfactant ABIL EM 90 (Evonik Industries, Essen, Germany).[30] Other chemicals used in the aqueous phase, potassium chloride (KCl), PEO (Mv 400 000), and glycerol, were all purchased from Sigma-Aldrich. Ultrapure water was used to prepare all solutions.

C. Digital LAMP

The LAMP cocktail was prepared using a LAMP kit with fluorescent dye (E1700, New England Biolabs, MA) according to the prescribed protocol. Lambda DNA (New England Biolabs, MA) was used as a template and serially diluted in 1X TE buffer using LoBind Tubes (Eppendorf, NY). The primers (IDT, IA) and concentration in the final cocktail were F3 (0.2M): 5-GGCTTGGCTCTGCTAACACGTT-3, B3 (0.2M): 5-GGACGTTTGTAATGTCCGCTCC-3, FIP (1.6M): 5-CAGCCAGCCGCAGCACGTTCGCTCATAGGAGATATGGTAGAGCCGC-3, BIP (1.6M): 5-GAGAGAATTTGTACCACCTCCCACCGGGCACATAGCAGTCCTAGGGACAGT-3, LoopF (0.8M): 5-CTGCATACGACGTGTCT-3, and LoopB (0.8M): 5-ACCATCTATGACTGT ACGCC-3.[31] The cocktail was supplemented with a final concentration of 1% PEO to assist droplet generation. To prevent evaporation during incubation and reduce the number of droplet transfer steps, droplets were produced in a modified 1.5 ml centrifuge tube (Eppendorf) with a drilled hole on its side wall to accommodate the micropipette. During droplet generation, the centrifuge tube was held vertically on a metal plate which served as the counter electrode. After droplet production was complete, the micropipette was removed and the hole was sealed with wax to ensure proper sealing during thermal incubation, which is held at 60 °C in an oven for 60 min with the tube cap closed. After incubation, the droplets were pipetted into a 96-well imaging plate (Sigma-Aldrich) and imaged with an inverted fluorescent microscope (Olympus IX71). The threshold was set at the average intensity between the brightest and dimmest droplets before processing and enumerating using ImageJ software.

III. RESULTS AND DISCUSSION

A. Monodispersed droplet generation with AC electric fields

Electrospray in air typically works at very high electric fields for mass spectrometry applications, such that a Taylor cone is formed to electrically discharge charged droplets with widely different radii. This droplet generation mode is often called tip streaming. At moderate electric field strengths, however, dripping becomes the dominant mode. It is well known that solutions with long polymeric molecules, such as PEO, form a filament at the nozzle and droplets are formed at the end of the filament.[32,33] For immersed electrospray operating in the dripping mode, this long filament offers two benefits: first, it prevents discharging by tip streaming from a Taylor cone; and second, the droplets are generated at the end of the filament, away from the high electric field region near the nozzle, to suppress field-induced coalescence.[34] Although both DC and AC fields have been used for electrohydrodynamic droplet generation, using AC can reduce the charge density on the liquid interface, therefore suppressing discharging during the filament formation stage after each droplet ejection event.[35] The frequency of the AC field is chosen so that it is close to the inverse RC time $f = D/d\lambda$ of the aqueous solution to reduce double layer charging, where D is the diffusivity of the major ions, d the tip diameter of the micropipette, and λ the ionic strength-dependent Debye length.[24,25] Invoking the Einstein-Stokes equation, the diffusivity D in 1% PEO solution will be smaller due to the viscosity increase.[36] As a result, f is estimated to be on the order of 5 kHz for 100 mM KCl solution in 1% PEO solution. The frequency of 10 kHz is used in all AC experiments in this paper. Experiments (not reported) at lower frequencies showed pronounced discharge due to high surface charge density and at higher frequencies showed significant droplet coalescence due to insufficient surface charging/whipping.

The experiments were carried out in the immersed electrospray setup described in the experimental section [Fig. 1(a)]. KCl was added to the aqueous solution to increase its conductivity. When using the 1% PEO solution as the dispersed phase, we found that the droplets were ejected from a filament jet near the tip, as shown in Fig. 1(b). The whipping filament exhibited a spiraling mode and seemed to eject two droplets per spiral. The ejected droplets formed a double helix downstream, as seen in Fig. 1(b). Some secondary satellite droplets were observed as the liquid in the filament cannot be completely drained by the droplets. However, microscopic images showed that the secondary droplets represent less than 0.1% of the total volume of generated droplets. This is consistent with our earlier analysis that viscoelastic additives favor the formation of filaments and suppress the formation of satellite droplets.[32] In contrast, Fig. 1(b) shows that without the PEO additives, satellite droplets constitute a large portion of the ejected droplets. The larger droplets also coalesce to form even larger droplets, thus creating highly dispersed suspensions of droplets. Since the dispersed phase is heavier than the continuous phase, the droplets settle to the bottom of the reservoir (Video S1). Using this setup, we can produce monodispersed droplets at the specific applied potential and pressure as shown in Figs. 1(c) and 1(d). The average diameter of the droplets was 50.2 μm with a coefficient of variation (CV) of 2.0%.

B. Effect of the PEO concentration on droplet monodispersity

Experiments with different PEO concentrations were tested with the same device. As the PEO concentration decreases below 0.5 wt. %, the filament becomes less visible and tip streaming becomes the dominant mode of droplet generation with very fine generated droplets. The critical concentration for monodispersed droplet generation falls near a critical PEO concentration C^+ of 0.5 wt. % that demarcates the diluted and the so-called "semi-dilute non-entangled" regime.[37] We believe that at a concentration higher than C^+, the entanglement and overlap in polymer solution facilitate the filament formation.[38] It is clear from the spray images of Fig. 2(a), frames ii to iv, that below C^+, satellite droplets constitute a large portion of the ejected droplets even if a filament is present. Large droplets with dimensions twice to 10 times of the average, which result from coalescence, are also apparent from the images of the settled droplets below the spray images. The satellite and coalesced droplets exhibit a dramatic decrease in

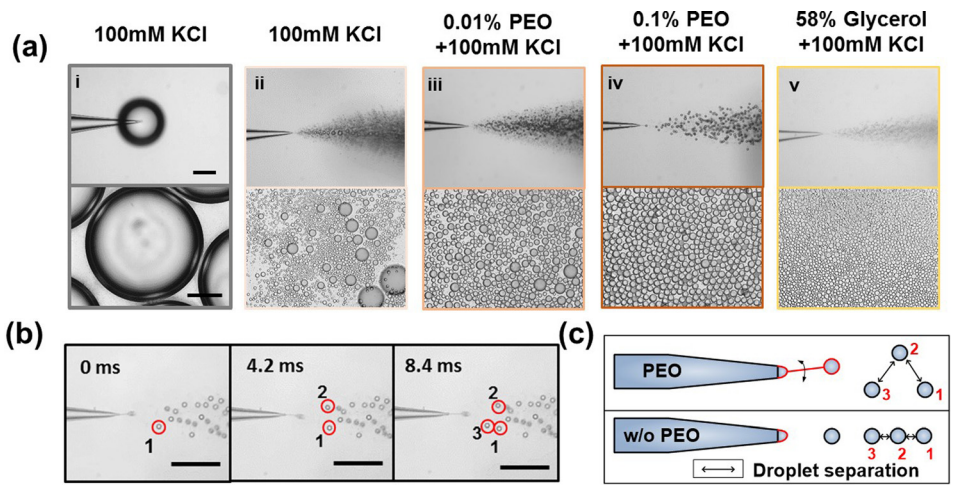

FIG. 2. (a) iACE behavior using various dispersed phases with different viscoelastic properties. Upper panels i–v: snapshots during droplet generation with dispersed phases of different PEO and glycerol concentrations. The same pressure of 2.9 kPa was applied for all experiments. No applied potential was used for frame (i); 480 V was used for experiments (ii)–(v); the scale bar is 500 μm. Lower panels (i)–(v): produced droplets at the bottom of the reservoir; the scale bar is 200 μm. Both panels show the disappearance of discharged and large droplets (due to coalescence) beyond a critical PEO concentration. (b) Snapshots of a high speed video showing AC droplet generation with an applied potential of 480V and a pressure of 2.9 kPa using a micropipette with a tip diameter of 18 μm. The scale bar is 200 μm. (c) Schematic of the effect of the whipping viscoelastic filament during droplet generation.

the number beyond C^+ just from visual inspection of Fig. 2(a). The viscoelasticity of the additive hence plays an important role in suppressing both events.

As a shear-thinning solution, PEO at 1% concentration has a viscosity that ranges from 12 to 3 mPa s.[37] To verify that the achieved monodispersity is due to the elasticity of the PEO solution and not the increased viscosity, non-viscoelastic glycerol solution with a viscosity of 12 mPa s was tested, as shown in Fig. 2(a). Tip streaming remains as the dominant mode of electrospray with glycerol, therefore eliminating viscosity as the mechanism for monodispersed droplet production in the iACE system. The elasticity of PEO suppresses the capillary instability of the filament and favors its formation over the tip-streaming Taylor cone.

To understand the droplet generation process of the iACE system, a high speed video was taken and shown in Fig. 2(b). A whipping and spiraling filament was observed at the tip, and droplets generated from the end of the filament appeared alternatively on different sides of the pipette axis to form the droplet double-helix downstream (Video S2). The off-axis staggered placement of droplets after their formation greatly increases the separation of droplets, in the all-important direction normal to the axis, compared to single-file alignment along the axis [Fig. 2(c)]. This normal separation minimizes field-induced coalescence. The length of the filament also places the droplets further from the tip where the electric field strength is high. The origin of this unique droplet generation mechanism can be attributed to an AC version of the whipping instability of the filament, commonly seen in DC electrospinning.[12,39]

C. DC verse AC field

The DC field was also tested using the same setup. When working in the DC mode, the growing meniscus at the orifice of the micropipette has a strong tendency to oscillate chaotically off axis, to the extent that a filament cannot be formed. This oscillation disappears with the AC field. The meniscus oscillation under DC is most likely due to side discharges from the meniscus, which give rise to non-monodispersed droplets. The electrostatic repulsion between highly charged droplets from the DC spray is evident from the out-of-focus droplets in Fig. S1. In the AC mode, however, the droplets are able to stay close to each other, suggesting that they are not strongly charged. The chaotic nature of the oscillating meniscus and the discharge droplet generation process in DC electrospray produce polydispersed droplets (Fig. S1) with CV $> 10\%$. Therefore, only the AC field is used in future experiments.

D. Effect of the ionic strength of the dispersed phase

As the electric field was focused to the water-oil interface due to the high electrical conductivity of the aqueous phase, the effect of which on iACE behavior was studied. We have measured the conductivity of the 100 mM KCl solution to be 1.0 S/m and have varied the conductivity by a factor of 10. This will change the inverse RC time, but, given that the frequency used is roughly equal or below the inverse RC time of this range of conductivities, we do not see any influence in the droplet formation. Our droplet generation technique is hence very suitable for generation of droplets from highly viscous and high ionic-strength physiological solutions.

E. Key operating parameters

The dependence of the electrospray behavior on the operating parameters was studied by varying the applied potential U_a and water-phase back pressure P_a plane within the four regimes I–IV in Fig. 3(a). If U_a and P_a are too high or too low, the stable droplet generation mechanism in regime II cannot be realized. Below a critical pressure threshold P_c, tip streaming from a Taylor cone dominates in regime I. In regime III, small droplets are generated at the tip due to insufficient drainage of the filament and undergo further disintegration (Rayleigh fission[40]) because of their high charge density. In regime IV, the filament whipping cannot produce enough separation between produced droplets to prevent coalescence. The whipping behavior depends on the surface charge density on the viscoelastic filament which is a function

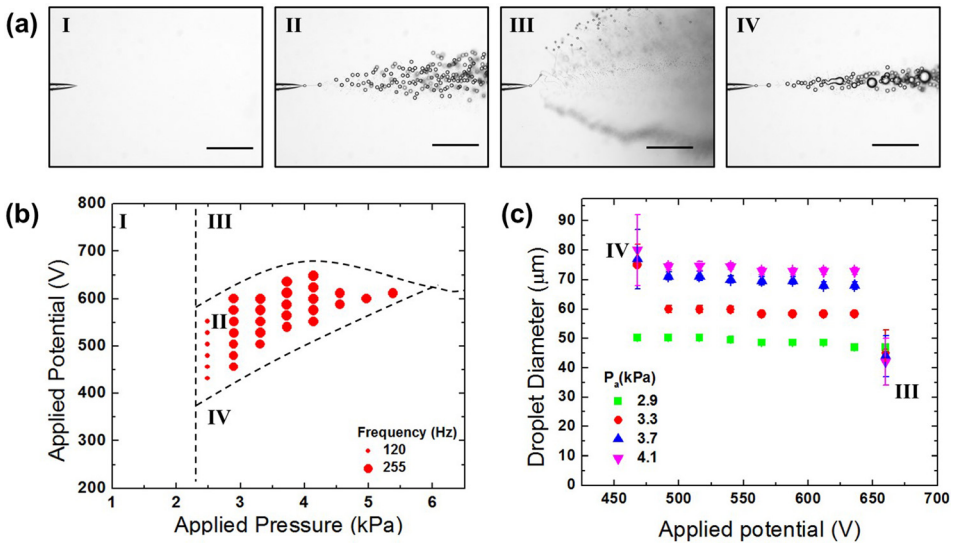

FIG. 3. (a) Representative snapshots of operating regimes I–IV for micropipettes with a tip diameter of 18 μm. The scale bar is 500 μm. (b) Operating regimes of applied potential and pressure for the same device as (a). Droplet generation frequency is expressed as the size of the dots. (c) Droplet size dependence on the applied potential at different applied pressures for the same device as (a). Data points belong to regime II with the limiting data in regimes III and IV indicated.

of filament dimension, ion conductivity, permittivity, flow rate, and electric field.[39] Therefore, the appropriate values of U_a and P_a need to be chosen for successful droplet production. The droplet generation frequency is studied in regime II. While the most data points show a generation frequency from 210 Hz to 255 Hz, a significantly lower frequency of 120 Hz is observed when P_a is near P_c. Nonetheless, we can draw the conclusion that U_a and P_a have little effect on the droplet generation frequency of the system when sufficient pressure is supplied.

The influence of applied potential on the droplet diameter was investigated with different applied pressures, as shown in Fig. 3(b). Within regime II, the droplet size decreases negligibly as U_a increases but remains monodispersed. P_a, however, almost doubles the droplet diameter within the stable area of operation in regime II. In regime III, when the meniscus undergoes fission due to a high interfacial charge density before a filament formed, a significant drop in the droplet size and an increase in polydispersity were observed. With a much lower U_a, field-induced coalescence increases both the droplet size and polydispersity. Therefore, all regimes except regime II were avoided in further experiments.

F. Control of the droplet size

Droplets of different sizes were generated from three micropipettes with different tip diameters d_t at different applied pressures, as shown in Figs. 4(a)–4(c). All droplet suspensions exhibited monodispersity with CVs smaller than 5%. Since the effect of U_a on the droplet size is weak, we focused on P_a as a relevant parameter for tuning the droplet size, even if it does not affect the droplet generation frequency. Within regime II, droplets increase in size as P_a increases for all d_t used. Micropipettes with larger tips produce droplets of larger diameter, as shown in Fig. 4(d). A model based on the pressure driven flow is used to capture the relationship between the droplet diameter and P_a and d_t. For a tapered conical micropipette with a small half cone angle α and a small ratio of tip to base diameter, a simple expression for its flow rate as a function of the pressure drop has been reported:[41]

$$Q = \frac{3\pi \tan \alpha}{64\mu}(P_a - P_c)d_t^3, \tag{1}$$

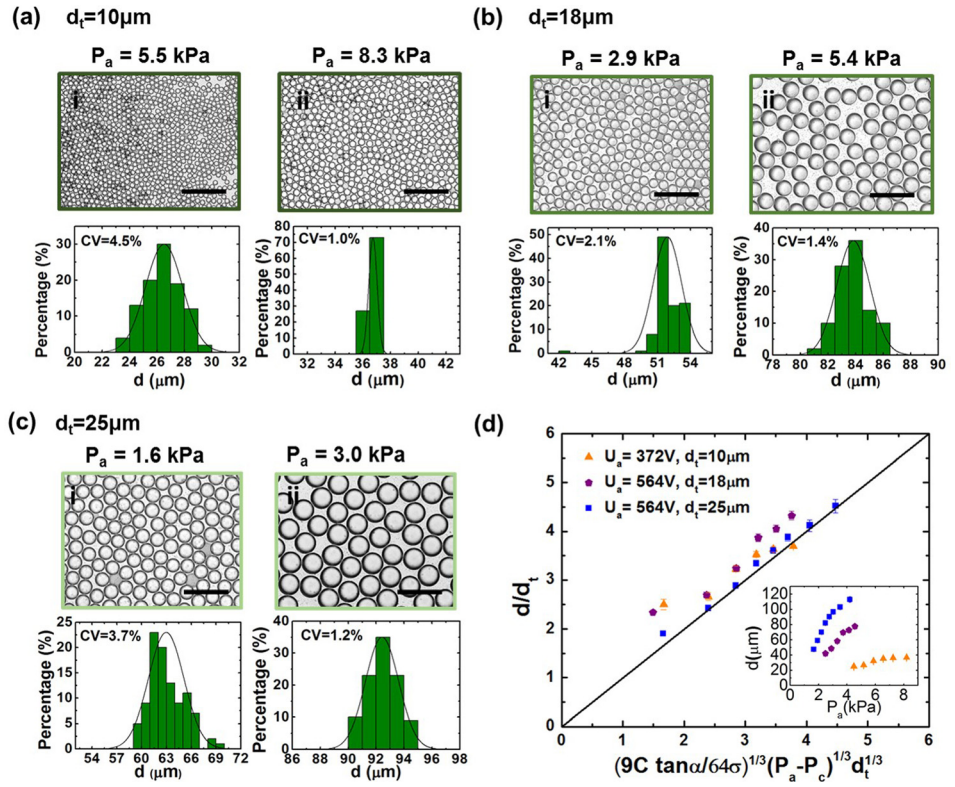

FIG. 4. (a)–(c) Monodispersed droplets produced from micropipettes with different tip diameters d_t. Applied potential U_a and pressure P_a used are as follows: (a) (i) 486V, 5.5 kPa and (ii) 576V, 8.2 kPa; (b) (i) 480 V, 2.9 kPa and (ii) 612V, 5.4 kPa; and (c) (i) 456V, 1.6 kPa and (ii) 576V, 3.0 kPa. The scale bar is 200 μm. (d) Droplet diameter scaled by tip diameter versus dimensionless parameter scaled by P_a and d_t. The inset shows unscaled droplet diameter versus applied pressure. $P_c = 4.1$ kPa is used for $d_t = 10$ μm, 2.3 kPa for $d_t = 18$ μm, and 1.5 kPa for $d_t = 25$ μm.

where Q is the flow rate, μ is the dynamic viscosity of the dispersed phase, and P_c is the critical pressure representing the boundary of the tip streaming regime I in Fig. 3, which represents the minimum threshold capillary pressure to eject fluid from the tip. The experimentally measured values of P_c were used in the equation.

On the other hand, the tip has a diameter of d_t and the characteristic capillary-viscous pinching time is $\tau = C\mu d_t/2\sigma$,[42] where C is a constant depending on the viscosity ratio between the dispersed and continuous fluids and σ is the surface tension between the two fluids. The formation time of the viscoelastic filament is omitted in this quasi-static approximation.[32,43] The final droplet volume is then expressed as $Q\tau$, which translates into a scaled relationship for the droplet diameter

$$d/d_t = (9C\tan\alpha/64\sigma)^{1/3}(P_a - P_c)^{1/3}d_t^{1/3}. \quad (2)$$

This relationship is used to collapse experimental data in Fig. 4(d) for micropipettes of different diameters and applied pressures. The conic pipette half angle α and the surface tension are measured to be 5° and 2.2 mN/m, respectively, and are used for all the data. The value of C is fitted to be 200, in good agreement with the values from previous theoretical studies of capillary pinch-off of a liquid jet in another immiscible fluid.[42,44] It corresponds to a viscosity ratio between 0.5 and 2, which is consistent with the fluids used here because of the shear-thinning effects of PEO.

It is clear from Fig. 4 and Eq. (2) that the droplet size is a function of both the back pressure and tip diameter. We are able to generate droplets from 40 μm to 100 μm in diameter for a tip diameter of 25 μm. Since the tip diameter can be adjusted from 1 μm to 50 μm, with the

lower bound limited by the Rayleigh fission limit and upper bound limited by the weakened field focusing effect on a large tip, we can in principle obtain monodispersed droplets with a diameter from 5 μm to 150 μm from different tips.

The fact that our droplet generation technology can adjust its droplet size by simply adjusting the back pressure, without delicate tuning of flow rates, allows us to disperse viscous physiological fluids into a precise number of droplets for accurate absolute quantification in digital PCR and LAMP.

G. Digital LAMP reaction

We performed LAMP reaction using iACE in a modified centrifuge tube, where the micropipette with a filament was placed through a drilled hole on its sidewall. During droplet generation, the filament is always wetted by a tiny amount of water which maintains an electrical connection between the electrode and the water phase even when they are not in visible contact in the final stage of the experiment. This phenomenon allows all reaction mix to be dispersed, leaving no dead volume. Stock lambda DNA solution was serially diluted in 1X TE buffer, which were further diluted 4.5 times when preparing the final reaction solution. Several researchers have performed digital LAMP in droplets[20,27,45] with varying amplification efficiencies from 2.6% to 100%. The large variation in amplification efficiency mostly comes from the different protocols performing the denaturing step of the template molecules before the amplification. In our experiments, we achieved the highest yield by immediately putting the denatured template solution in ice (within seconds) after heating it at 85 °C for 2 min. This protocol was hence used for all template concentrations. For each concentration, 20 μl solution was dispersed into 55 pl droplets in 15 min using iACE. After incubation, the droplets have settled to the bottom of the centrifuge tube and were manually transferred to a imaging well with a pipette. Care was taken during transfer to allow spreading of droplets and to avoid droplet coalescence. After the droplets settled down in the imaging well and formed a monolayer, images were taken to analyze the fluorescence intensity of about 1000 droplets for each concentration (see Fig. 5). The percentage of droplets P with intensity above a certain threshold was used to calculate μ, the average template copy number per droplet, from the Poisson distribution $\mu = -\ln(1 - P)$. The estimated template concentration was obtained by dividing μ by the average droplet volume. We achieved an efficiency of 53% with iACE and good linearity ($R^2 = 0.999$) between the added and the measured target concentrations.

IV. CONCLUSION

We have demonstrated a novel monodispersed water-in-oil droplet generation method using AC electrospray. Common issues associated with an immersed electrospray setup, such as discharge and droplet coalescence, were avoided by the addition of a biocompatible and viscoelastic polymer (PEO) into the aqueous phase. PEO forms a whipping filament which prevents Taylor cone formation and ejects separated drops away from the high-field tip region. We showed easy tuning of the droplet diameter from 25 μm to 100 μm by adjusting the back pressure, which can be guided by a convenient scaling correlation. The benefit of using AC instead of DC electric fields is not only better monodispersity but also less electrical damage to the molecules within the aqueous solution. The setup was successfully applied to absolute nucleic acid quantification using LAMP, with good amplification efficiency and linear correlation with respect to the added template concentration.

Flow-free water-in-oil droplet generation is attractive because it allows easy tuning of the droplet diameter and simple parallelization for high throughput applications. Moving away from a microfluidic chip design without micropumps should also lower the product cost. These advantages are particularly pertinent for large-scale parallelized production of droplets from a viscous dispersed phase, which has become important in many current and future applications.

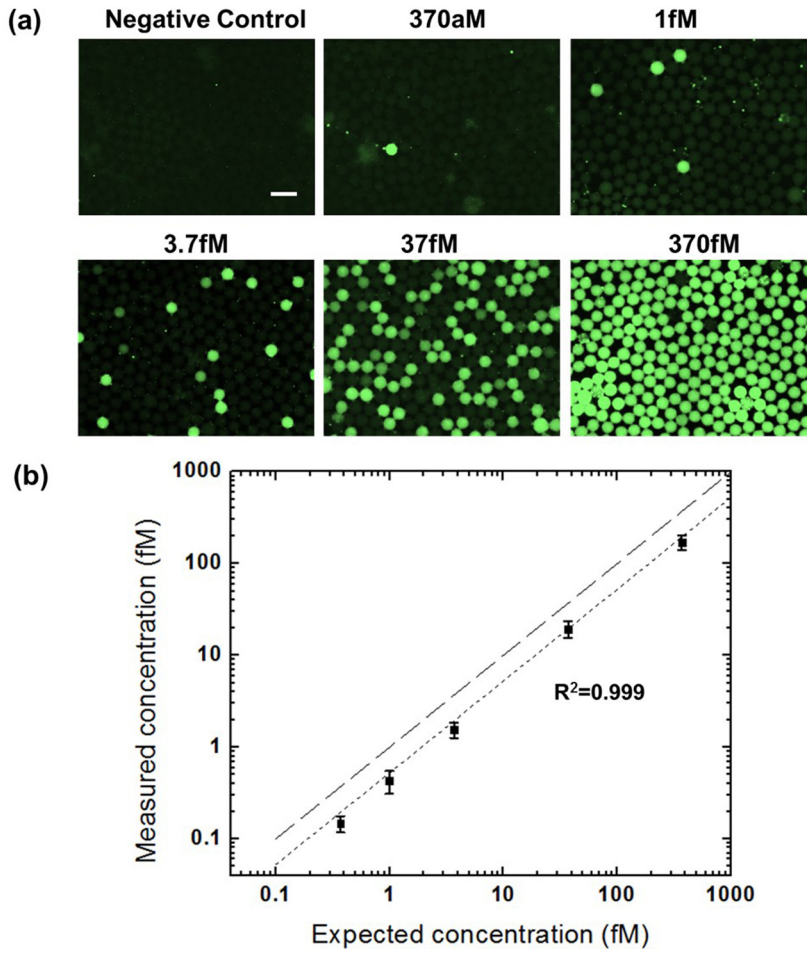

FIG. 5. (a) Fluorescent image of droplets after LAMP reaction at different target concentrations. The scale bar is 100 μm. (b) Calibration curve of the droplet concentration. Short dashed line: linear fit to experimental data and long dashed line: ideal calibration curve. Triplicate experiments were carried out at each template concentration.

SUPPLEMENTARY MATERIAL

See supplementary material for images of DC electrospray showing meniscus oscillations while spraying from the tip due to excessive charging, which generates non-monodispersed droplets, and videos showing droplets settling down to the bottom of the chip and whipping due to the viscoelastic filament.

ACKNOWLEDGMENTS

Z.P. is grateful for a fellowship from the Chinese Scholarship Council and useful advice from Dr. Ceming Wang while drafting this paper. This research was supported by the Bayer Chair discretionary fund to H.C.C.

[1]A. J. deMello, Nature **442**, 394 (2006).
[2]R. Zilionis, J. Nainys, A. Veres, V. Savova, D. Zemmour, A. Klein, and L. Mazutis, Nat. Protoc. **12**, 44 (2017).
[3]C. M. Hindson, J. R. Chevillet, H. A. Briggs, E. N. Gallichotte, I. K. Ruf, B. J. Hindson, R. L. Vessella, and M. Tewari, Nat. Methods **10**, 1003 (2013).
[4]S. M. Prakadan, A. K. Shalek, and D. A. Weitz, Nat. Rev. Genet. **18**, 345 (2017).
[5]R. K. Shah, J.-W. Kim, J. J. Agresti, D. A. Weitz, and L.-Y. Chu, Soft Matter **4**, 2303 (2008).
[6]T. Thorsen, R. W. Roberts, F. H. Arnold, and S. R. Quake, Phys. Rev. Lett. **86**, 4163 (2001).
[7]P. Umbanhowar, V. Prasad, and D. Weitz, Langmuir **16**, 347 (2000).
[8]A. Utada, E. Lorenceau, D. Link, P. Kaplan, H. Stone, and D. Weitz, Science **308**, 537 (2005).
[9]S. L. Anna, N. Bontoux, and H. A. Stone, Appl. Phys. Lett. **82**, 364 (2003).

[10]P. Garstecki, H. A. Stone, and G. M. Whitesides, Phys. Rev. Lett. **94**, 164501 (2005).
[11]J. D. Wehking, M. Gabany, L. Chew, and R. Kumar, Microfluid. Nanofluid. **16**, 441 (2014).
[12]J. Guerrero, J. Rivero, V. R. Gundabala, M. Perez-Saborid, and A. Fernandez-Nieves, Proc. Natl. Acad. Sci. **111**, 13763 (2014).
[13]E. Castro-Hernández, P. García-Sánchez, J. Alzaga-Gimeno, S. H. Tan, J.-C. Baret, and A. Ramos, Biomicrofluidics **10**, 043504 (2016).
[14]J. Zeng and T. Korsmeyer, Lab Chip **4**, 265 (2004).
[15]S. H. Tan, B. Semin, and J.-C. Baret, Lab Chip **14**, 1099 (2014).
[16]S. J. Kim, Y.-A. Song, P. L. Skipper, and J. Han, Anal. Chem. **78**, 8011 (2006).
[17]A. Barrero, J. Lopez-Herrera, A. Boucard, I. Loscertales, and M. Marquez, J. Colloid Interface Sci. **272**, 104 (2004).
[18]S. Jayasinghe, J. Microencapsulation **24**, 430 (2007).
[19]B. Sharma, Y. Takamura, T. Shimoda, and M. Biyani, Sci. Rep. **6**, 26257 (2016).
[20]P. Xu, X. Zheng, Y. Tao, and W. Du, Anal. Chem. **88**, 3171 (2016).
[21]M. Zagnoni, G. Le Lain, and J. M. Cooper, Langmuir **26**, 14443 (2010).
[22]R. B. Karyappa, A. V. Naik, and R. M. Thaokar, Langmuir **32**, 46 (2015).
[23]H. Yan, L. He, X. Luo, J. Wang, X. Huang, Y. Lü, and D. Yang, Langmuir **31**, 8275 (2015).
[24]L. Y. Yeo, D. Lastochkin, S.-C. Wang, and H.-C. Chang, Phys. Rev. Lett. **92**, 133902 (2004).
[25]M. Z. Bazant, K. Thornton, and A. Ajdari, Phys. Rev. E **70**, 021506 (2004).
[26]Y. Hu, P. Xu, J. Luo, H. He, and W. Du, Anal. Chem. **89**, 745 (2016).
[27]B. Sun, F. Shen, S. E. McCalla, J. E. Kreutz, M. A. Karymov, and R. F. Ismagilov, Anal. Chem. **85**, 1540 (2013).
[28]T. Notomi, H. Okayama, H. Masubuchi, T. Yonekawa, K. Watanabe, N. Amino, and T. Hase, Nucl. Acids Res. **28**, e63 (2000).
[29]R. Fiammengo, Biomarkers Med. **11**, 69 (2017).
[30]Z. Chen, P. Liao, F. Zhang, M. Jiang, Y. Zhu, and Y. Huang, Lab Chip **17**, 235 (2017).
[31]N. A. Tanner, Y. Zhang, and T. C. Evans, Jr., Biotechniques **53**, 81 (2012).
[32]H.-C. Chang, E. A. Demekhin, and E. Kalaidin, Phys. Fluids **11**, 1717 (1999).
[33]V. Tirtaatmadja, G. H. McKinley, and J. J. Cooper-White, Phys. Fluids **18**, 043101 (2006).
[34]A. R. Thiam, N. Bremond, and J. Bibette, Phys. Rev. Lett. **102**, 188304 (2009).
[35]N. Chetwani, S. Maheshwari, and H.-C. Chang, Phys. Rev. Lett. **101**, 204501 (2008).
[36]A. Einstein, Ann. Phys. **324**, 371 (1906).
[37]K. W. Ebagninin, A. Benchabane, and K. Bekkour, J. Colloid Interface Sci. **336**, 360 (2009).
[38]M. G. McKee, G. L. Wilkes, R. H. Colby, and T. E. Long, Macromolecules **37**, 1760 (2004).
[39]M. M. Hohman, M. Shin, G. Rutledge, and M. P. Brenner, Phys. Fluids **13**, 2201 (2001).
[40]D. Duft, T. Achtzehn, R. Müller, B. A. Huber, and T. Leisner, Nature **421**, 128 (2003).
[41]L. C. Cerny and W. P. Walawender, Bull. Math. Biophys. **28**, 11 (1966).
[42]H. A. Stone and L. Leal, J. Fluid Mech. **198**, 399 (1989).
[43]J. Cooper-White, J. Fagan, V. Tirtaatmadja, D. Lester, and D. Boger, J. Non-Newtonian Fluid Mech. **106**, 29 (2002).
[44]T. R. Powers, D. Zhang, R. E. Goldstein, and H. A. Stone, Phys. Fluids **10**, 1052 (1998).
[45]F. Schuler, M. Trotter, M. Geltman, F. Schwemmer, S. Wadle, E. Domínguez-Garrido, M. López, C. Cervera-Acedo, P. Santibáñez, F. von Stetten, R. Zengerle, and N. Paust, Lab Chip **16**, 208 (2016).